Article

Silica-Titania Integrated Photonics Platform-Based 1 × 2 Demultiplexer Utilizing Two Serially Cascaded Racetrack Microrings for 1310 nm and 1550 nm Telecommunication Wavelengths

Muhammad A. Butt *[ID], **Muhammad Shahbaz, Łukasz Kozłowski, Andrzej Kaźmierczak** [ID] **and Ryszard Piramidowicz** [ID]

Institute of Microelectronics and Optoelectronics, Warsaw University of Technology, ul. Koszykowa 75, 00-662 Warszawa, Poland
* Correspondence: ali.butt@pw.edu.pl

Abstract: Herein, a numerical analysis of a 1 × 2 demultiplexer based on a silica-titania integrated photonics platform is conducted via the finite element method. The structure is composed of two coupled racetrack microrings (RTMRs) and a subwavelength grating (SWG) structure for the demultiplexing of 1310 nm and 1550 nm telecommunication wavelengths. The material platform selected for this design is highly attractive due to its refined optical, physical, and chemical properties. Moreover, silica-titania sol-gel thin-films can be deposited on glass substrates with the dip-coating method. The proposed device has a small footprint of 84×125 μm^2 and offers crosstalk as low as ~ -6.6 dB and ~ -9.04 dB for 1550 nm and 1310 nm, respectively. We are convinced that this study promotes the use of the silica-titania platform for the development of low-cost on-chip optical communication devices for signal multiplexing and demultiplexing.

Keywords: demultiplexer; silica-titania platform; racetrack microrings; subwavelength grating structure; telecommunication wavelength; wavelength division multiplexing

1. Introduction

In optical communication networks, the concept of using light waves to convey data and information packets provides great benefits including high speed, high bandwidth, electro-magnetic immunity, etc. [1]. The optical fibers act as the transmission channel for optical waves in optical communication networks [2]. The effective capacity of optical fibers has subsequently been maximized using wavelength division multiplexing (WDM) technology [3,4] such that several users can share a single (physical) optical fiber and various (data) optical channels can be sent over the same single optical fiber. To distinguish these channels from one another and send them to their appropriate users, a proper photonic device is required at the user end of the network. Mach-Zehnder interferometers (MZI) [5,6], multimode interference (MMI) couplers [7–9], Y-branch devices [10,11], ring resonators [12–15], and other solutions can all be used to create optical demultiplexers based on different optical platforms, which are a crucial components of communication networks [16–19]. Moreover, small size and low crosstalk demultiplexer devices may have advantages in quantum information processing and quantum communication [20–22].

Recently, several novel demultiplexer system designs have been proposed on semiconductor platforms. For instance, a novel design of an 8-channel MMI demultiplexer utilizing slot waveguide (WG) structures that operate at 1530 nm, 1535 nm, 1540 nm, 1545 nm, 1550 nm, 1555 nm, 1560 nm, and 1565 nm was proposed [23]. The device is composed of Gallium nitride (GaN) with silicon (Si) surrounding it and constructed using seven 1 × 2 MMI couplers, 14 S-bands, and 1 input taper. The geometrical parameters

were analyzed using a full vectorial-beam propagation method (FV-BPM), and simulation results show that the device has low crosstalk (CT) (−19.97−−13.77 dB) and bandwidth (1.8–3.6 nm) and can transmit 8-channels across the entire C-band (1530–1565 nm). Another work on MMI suggested a design for an optical demultiplexer utilizing slot-WG technology that can operate at wavelengths of 547 nm, 559 nm, 566 nm, and 584 nm [24]. The use of GaN and silicon oxide in the slot-WG structure was found to be beneficial. Simulation results indicate the device has low transmission loss (0.983–1.423 dB), minimal CT (13.8–18.3 dB), and wide bandwidth (1.8–3.2 nm), making it suitable for use in WDM visible light networking systems.

A 5-channel DWDM demultiplexer design using photonic crystal (PhC) hexagonal ring resonators (RRs) of airholes on a silicon slab as channel drop filters is presented [25], along with an analysis of its optimal design parameters and device performance. Wavelength control is achieved through fine-tuning coupling holes outside each ring resonator, resulting in resolved wavelengths in the range of 1535 to 1539 nm, suitable for use with erbium doped fiber amplifiers. The average coupling efficiency and CT were found to be 72.4% and −18.31 dB, respectively. In [26], a five-channel demultiplexer utilizing a simple ring resonator is proposed for the third communication window 1550–1567 nm range. The resonant wavelengths in the output ports were adjusted by altering the dielectric constant of the ring core. According to the study, this demultiplexer structure is suitable for use in WDM optical communication systems. The CT between channels was calculated, with a maximum value of −13 dB and a minimum of −24 dB. The average transmission efficiency is above 92%, with channel spacing of less than 4.2 nm and an average bandwidth of less than 1.51 nm. The quality factor for the channels ranges from 1034 to 1044. The overall size of the demultiplexer is roughly 689.61 μm^2, which according to the authors makes it practical for use in optoelectronic and photonic integrated circuits.

An ultra-compact wavelength demultiplexer operating at O-band (~1310 nm) and C-band (~1550 nm) is proposed using a subwavelength grating (SWG) [27]. The proposed scheme utilizes the SOI platform, utilizing silicon WGs (with a refractive index of approximately 3.478) on a SiO_2 substrate (with a refractive index of approximately 1.455) with a thickness of 2 μm. The device is fully embedded in a silicon oxide cladding. The device also has a wide 1-dB bandwidth of 140 nm across the O-band and 125 nm across the C-band, with low insertion losses of 0.27 dB and 0.08 dB for the central wavelength of 1310 nm and 1550 nm, respectively, and an extinction ratio of better than 15 dB for both central wavelengths. The device is more sensitive to fabrication errors in the gap between the strip WGs of a DC, as it has a greater impact on the effective refractive index of the first TE modes.

Furthermore, a compact and broadband WDM utilizing an SWG-assisted directional coupler was developed and successfully tested for separating wavelengths of 1310 nm and 1550 nm on an SOI platform [28]. The inclusion of an SWG allows for a greatly reduced size, achieved through precise phase matching at 1550 nm and a large phase mismatch at 1310 nm. The final device offers high extinction ratios (ER) of 23 dB and 19 dB at 1310 and 1550 nm, respectively, with 3-dB bandwidths of 85 nm for the O-band (ER >15 dB) and 140 nm for the C-band (ER > 10 dB). A grating coupler for fiber-chip connections based on SOI that can split wavelengths for both O and C communication bands without being affected by polarization is proposed in [29]. This was achieved by using subwavelength segmentation of silicon gratings and a special design that allows dual wavelengths to travel in opposite directions on the chip. The coupler's efficiency for TE and TM polarizations was around −4.5 dB at both 1310 nm and 1550 nm, with an average 1-dB bandwidth of ~45 nm and ~60 nm, respectively. An AWG demultiplexer using Si photonic WGs was demonstrated in [30]. The researchers designed and fabricated a 110 × 93 mm^2 AWG on an SOI platform, with a demultiplexing function observed in the wavelength range of 1500–1570 nm, a channel spacing of 6 nm, and a free spectral range of over 90 nm. The study also suggested that a channel spacing of 1 nm could be achieved in an area of 500 mm^2 through the optimization of AWGs and slab WGs. An optical demultiplexer

with a 1 × 4 channel configuration was proposed using an ultra-low-loss Si_3N_4 WG with a propagation loss of approximately 3.1 dB/m [31]. It includes three 2 × 2 MZIs, each containing two 2 × 2 multimode interference couplers based on general interference. The couplers have power division ratios of −3.3 dB to −3.7 dB across a 50 nm wavelength range of 1530 nm to 1580 nm. The demultiplexer is thermally tunable, with chrome-based heaters on the delay arms of the MZI filters to control the optical phase shift and achieve a moderately low CT of 14.5 dB between adjacent channels. The insertion loss per channel is between 1.5 dB and 2.2 dB in the 1550 nm to 1565 nm wavelength range.

Inspired by the previously demonstrated demultiplexer configurations, herein, a 1 × 2 demultiplexer based on two serially cascaded racetrack microrings is proposed. The selection of the silica-titania platform is based on our ongoing project on the development of low-cost photonic devices [32]. The initial, very promising results related to the deposition of high-quality WG films via the dip-coating method are obtained. In this work, we reported the numerical modeling study of the demultiplexer device based on the silica-titania platform and fabrication methods that will be employed in the final implementation of this device.

2. Silica-Titania Platform

The choice of an appropriate material for the previously mentioned structures is one of the most important aspects of the initial stage of the fabrication process. There are a number of options to choose from; however, we would like to emphasize the use of silica-titania $(SiO_2:TiO_2)$ as the WG material. $SiO_2:TiO_2$ is a material that has many possibilities in the field of photonic integrated circuits, because of its advantages [33] over other more conventional materials, for example, SiN or InP. The most convincing benefits of using $SiO_2:TiO_2$ are listed [34] in Figure 1.
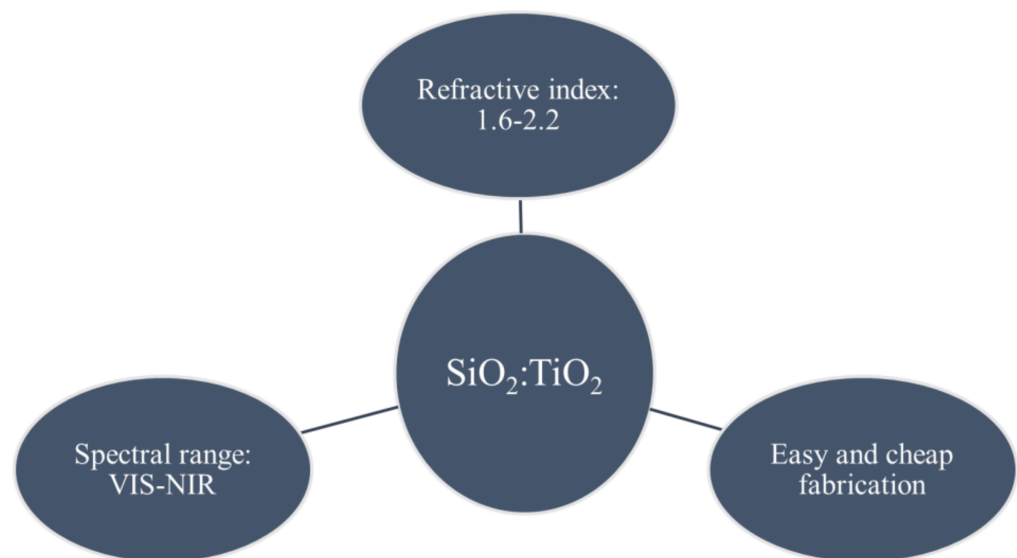
Figure 1. Main characteristics of $SiO_2:TiO_2$ platform.

This platform can be relatively easily manufactured by applying a thin-film of $SiO_2:TiO_2$ on a simple glass substrate. The preferred and simple method for $SiO_2:TiO_2$ film deposition is sol-gel dip-coating. The method itself is very easy to conduct and does not require any advanced equipment such as chemical vapor deposition (CVD) devices. It can be considered a great method for laboratory applications; however, it is not yet automatized, and it needs to be more developed to use for commercial purposes. Sol-gel dip-coating is conducted by dipping the substrate in the sol to be covered by the material; afterward, the substrate is withdrawn from the sol at a selected withdrawal speed and after the solvent evaporation, the thermal annealing process is conducted [35]. The process order is described in Figure 2.
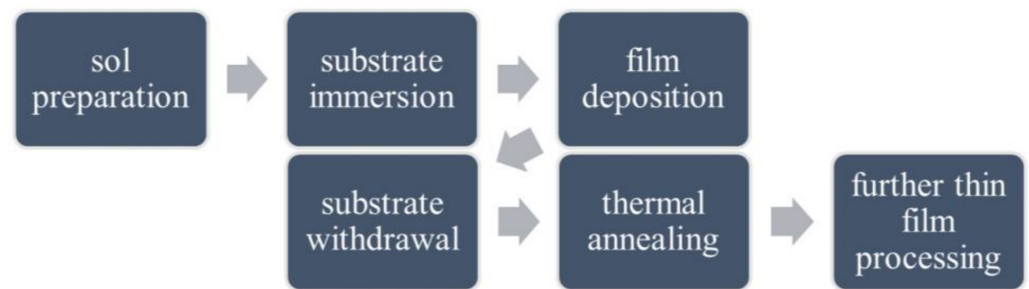
**Figure 2.** Graphical illustration of the sol-gel dip-coating method.

During the sol preparations, the used precursors are tetraethyl orthosilane $Si(OC_2H_5)_4$ (TEOS) and tetraethoxytitanate $Ti(OC_2H_5)_4$ (TET) for Si and Ti, respectively. First, partial hydrolysis of the solutions occurs, then they are mixed, and a homogenizing agent (ethyl) and catalyst (HCl) are added [36]. The obtained thin film is further processed to create waveguiding structures. In some special cases, the guiding structures are previously prepared in the substrate, for example, the reverse rib structures.

3. Fabrication Processes Under-Development

The next step after thin-film deposition is transferring the layout of previously designed structures to the prepared material sample. There are several technological solutions used to fabricate waveguiding structures in $SiO_2:TiO_2$ currently being considered by our consortium. We propose to take a deeper look at the following:

- Electron-beam (E-beam)/deep UV (DUV) lithography, combined with inductively coupled plasma—reactive ion etching (ICP-RIE)
- Optical lithography combined with wet chemical etching
- Nano-imprint lithography (NIL)

All of the three above-mentioned technological approaches differ from each other significantly in terms of fabrication cost and effort, as well as expected photonic circuit compactness. This is therefore a big advantage of using $SiO_2:TiO_2$, that all of them can be applied. It allows taking different approaches regarding fabrication. The comparison of these techniques is shown in Figure 3. ICP-RIE is a well-known and developed fabrication method for integrated photonics. It finds application with other materials such as SOI and InP platforms. However, it is expensive, difficult to carry, and requires advanced equipment and facilities. Nevertheless, using ICP-RIE gives nearly complete certainty of a successful fabrication [37].
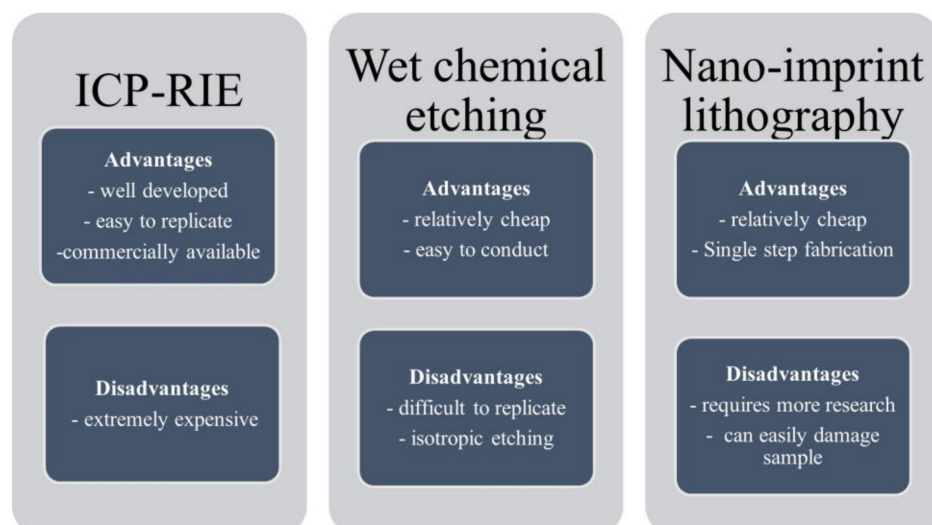
Figure 3. Pros and cons of the proposed fabrication method on the $SiO_2:TiO_2$ platform.

However, less developed methods such as wet chemical etching and NIL also deserve to be considered as potential fabrication techniques. Both chemical etching and NIL are relatively cheap and do not require advanced equipment or facilities. Those technologies combined with sol-gel dip-coating could result in a novel cheap approach to photonic integrated circuits fabrication. Wet chemical etching involves covering the substrate with a mask by photolithography, chemical etching with an acid solution (e.g., HF), and mask removal [38].

NIL is an etch-less fabrication method. It requires the previous fabrication of a "master stamp" and imprinting it over the deposited non-hardened WG film before the thermal annealing to form the structures [7]. However, both wet chemical etching and NIL are still under development for the SiO_2:TiO_2 platform and give a less probable successful fabrication effect than ICP-RIE.

4. Device Design and Numerical Model

The proposed 1×2 demultiplexer is based on double racetrack microring (RTMR) architecture, whereby two RTMRs are mutually coupled. Consequently, as each RTMR reverses the dropping direction concerning the optical signal input direction, the output of a double RTMR is acquired in the same direction as the input. The input signal, inserted into the input port is coupled to the 1st RTMR, which circulates along the racetrack circumference. When the wavelength of the inserted signal meets the resonance condition, the light is fully decoupled to the racetrack from the input WG and is decoupled to the 2nd racetrack. Following loops around the first ring couple, the two microrings together pass the light into the second microring once it reaches the resonance state of the second ring. Eventually, the light transfers into the output WG using the same technique as shown in Figure 4.
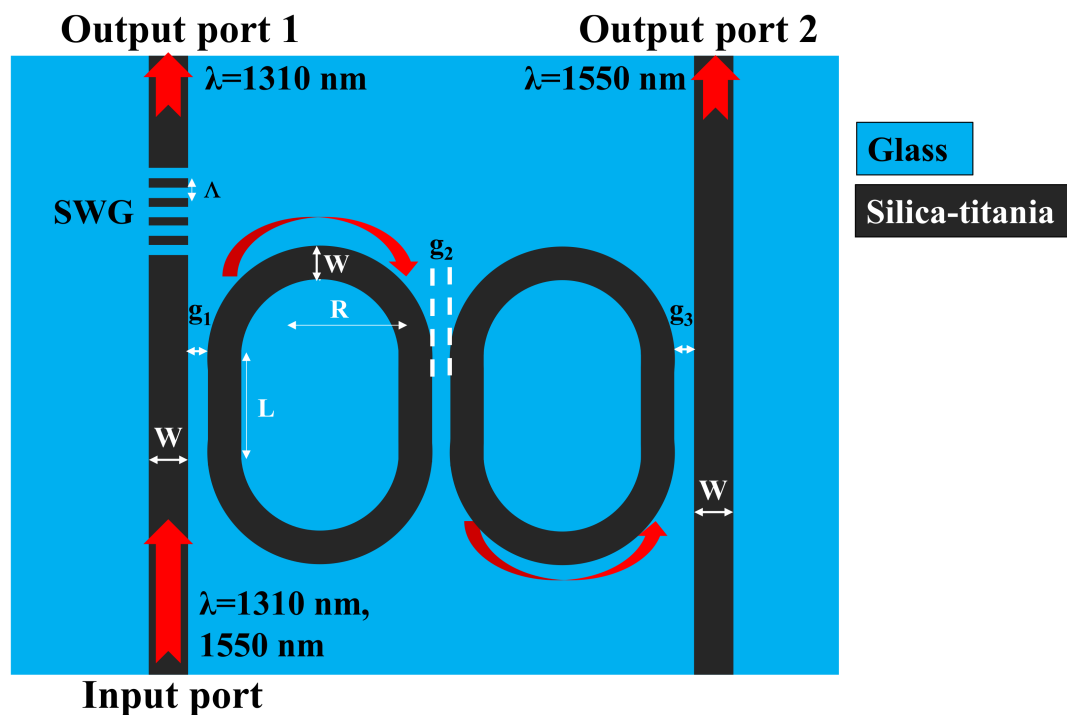
Figure 4. Schematic representation of 1×2 demultiplexer based on silica-titania RTMR structures and SWG segments for 1310 nm and 1550 nm telecommunication wavelength.

The radius of the RTMRs is devised in such a way that an operational wavelength of 1550 nm is coupled to a first RTMR and then transfers the power to the second RTMR and eventually, the output is collected at output port 2. The wavelength of 1310 nm can pass through the output port 1 without meeting the resonance condition of RTMR and thus

not being de-coupled to the ring. To obtain an enhanced working device, the geometric parameters such as the radius of the ring and coupling gaps should be properly optimized. The radius of the RTMR is denoted as R, which is identical for both rings; and L is the coupling length, which is fixed at 10 μm. The width of the bus WG and the ring WG is denoted as W. The geometry of the SiO_2:TiO_2 ridge WG is optimized for the single mode operation at the operational wavelength of 1310 nm and 1550 nm. The height of the WG is fixed at 400 nm, which can be obtained by performing the dip-coating method twice [34]. The W of the WG is varied between 1000 nm and 2500 nm, as shown in Figure 5. For λ = 1310 nm, the WG supports a single mode for W = 1000 nm to 1800 nm. For W > 1800 nm, multimode starts to appear. Whereas W < 1800 nm is a cut-off region for λ = 1550 nm. And the WG supports single mode till W = 2500 nm. Keeping in mind the single mode operation of both λ = 1310 nm and λ = 1550 nm, W = 1800 nm is the viable dimension for designing the optical WGs for the demultiplexer. The effective refractive indices of 1.5194 and 1.4742 are employed in the design for the wavelength of 1310 nm and 1550 nm, respectively.
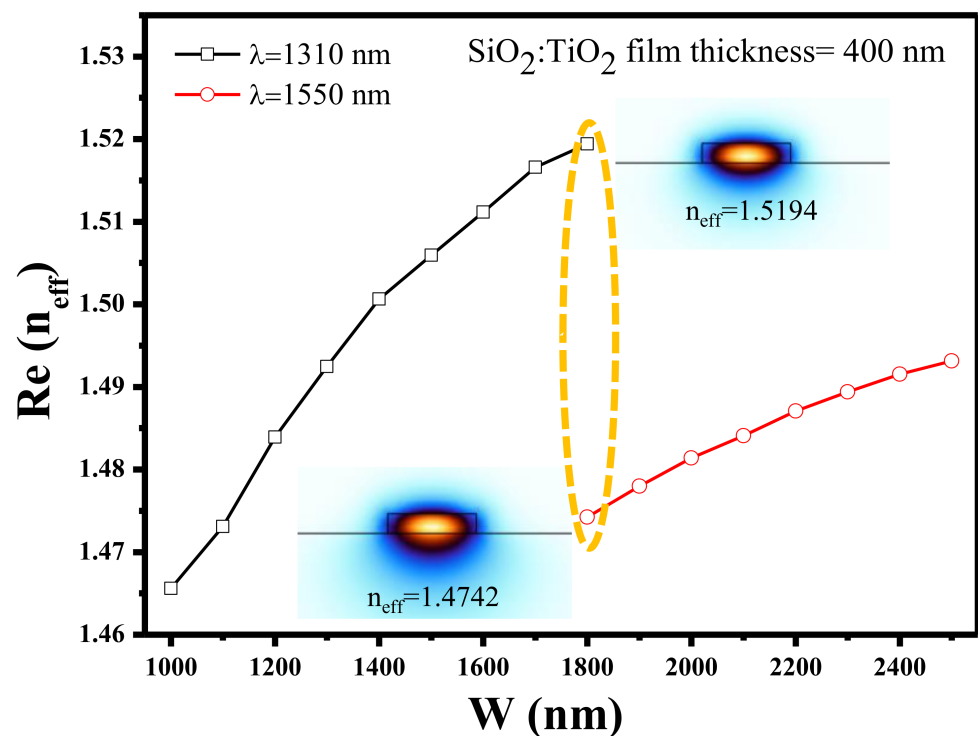

Figure 5. Real part of the effective refractive index of SiO_2:TiO_2 WG with varying W for the operational wavelength of 1310 nm and 1550 nm. The core height is fixed at 400 nm.

The coupling gap between the bus WG and the first RTMR, coupling gap between the first RTMR and second RTMR, and coupling gap between the second RTMR and drop port is denoted as g_1, g_2, and g_3, respectively. COMSOL Multiphysics software is being used to carry out the numerical analysis utilizing the finite element method (FEM). As a physics interface, the electromagnetic wave frequency domain (EWFD) has been used. In the whole demultiplexer design, the sub-domains in the WG cross-section are divided into triangular mesh components with a mesh grid size of λ/100. To simulate an open geometry, scattering boundary conditions (SBCs) are placed at the FEM simulation window's outside edges. To minimize the CT (dB) between the output ports, subwavelength grating (SWG) structures are introduced in the structure. The detailed geometric parameters of the device are shown in Table 1.

Table 1. Geometric parameters of the 1 × 2 demultiplex based on the silica-titania platform for 1310 nm and 1550 nm telecommunication wavelengths.

Parameter	Values
W	1800 nm (fixed)
R	10–22 μm (range)
L	10 μm (fixed)
g_1	80–180 nm (range)
g_2	80–370 nm (range)
g_3	60–120 nm (range)
Operational wavelength	1310 and 1550 nm (fixed)
Footprint	84 μm × 125 μm
$\Lambda = a + b$, where $b = 250$ nm	350–850 nm (range)
N	15

With numerous practical devices based on subwavelength structures, recent advancements in lithographic techniques on the semiconductor-on-insulator substrate with sub-10 nm patterning precision have gained recognition [39]. The three methodologies for the fabrication processes include lithography-based approaches, mechanics-enabled approaches, and post-trimming approaches. Despite being still widely used, lithography-based methods have low resolution and are expensive. With the advantages of better resolution or lower cost, mechanics-enabled and post-trimming technologies provide innovative alternatives that complement lithography-based approaches, particularly for applications in basic research and non-CMOS device manufacturing [39]. The essence of an SWG structure is a periodic arrangement of two distinct materials with a period significantly smaller than the wavelength of light [40]. The capability of SWG structures to do refractive index engineering is of ever-increasing interest. Light traveling in an SWG WG excites a mixture of the periodic structure's Bloch modes. Bloch waves are the natural modes of periodic media, just as plane waves are the inherent modes of free space. The Bloch mode has a wave vector of $k = 2\pi/\lambda$ and a temporal frequency of ω, and it propagates in the direction perpendicular to the periodic segments of SWG WG. The wavelength range that satisfies the equation $\Lambda = \lambda/2$ is regarded as a photonic bandgap (PBG) where there is no light transmission. The SWG WG segment is designed for the fill factor (FF = a/Λ) of 0.3 to 0.7, which provides a PBG for 1550 nm; and Bloch mode at 1310 nm can propagate as shown in Figure 6a. The E-field distribution in the SWG for FF = 0.61 at 1550 nm and 1310 nm is also presented in Figure 6b,c, respectively.
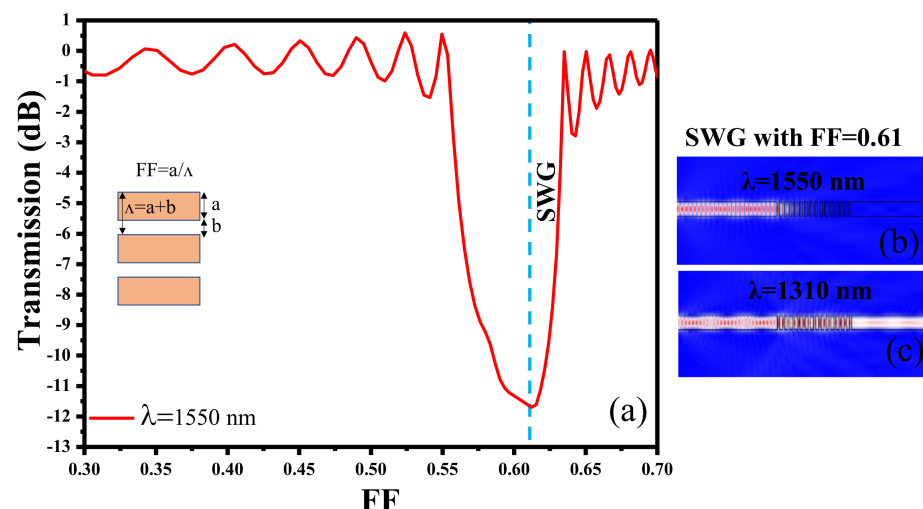
Figure 6. (**a**) Transmittance of SWG WG at varying FF for the operational wavelength of 1550 nm, (**b**) E-field distribution at λ = 1550 nm for SWG with FF = 0.61, (**c**) E-field distribution at λ = 1310 nm for SWG with FF = 0.61.

The 1 × 2 demultiplexer design is optimized step-by-step to obtain the maximum power coupling and lower CT (dB). In the first step, the optical confinement in the ring of different radiuses (R) at λ = 1310 nm and 1550 nm is analyzed. R is varied in the range of 10 μm and 22 μm whereas g_1 is fixed at 100 nm (as a starting point). From Figure 7a, it can be seen that the maximum optical confinement in the ring for λ = 1310 nm and λ = 1550 nm is obtained at R = 16.75 μm and R = 16 μm, respectively. This suggests that ΔR = 0.75 μm, which is quite big; therefore, the ring designed for λ = 1550 nm will not resonate at λ = 1310 nm. However, according to the equation $m\lambda = 2\pi R n_{eff}$, lower order resonant modes (m) can provide some mode power that can be blocked by inserting SWG structures in the thru port [40,41].
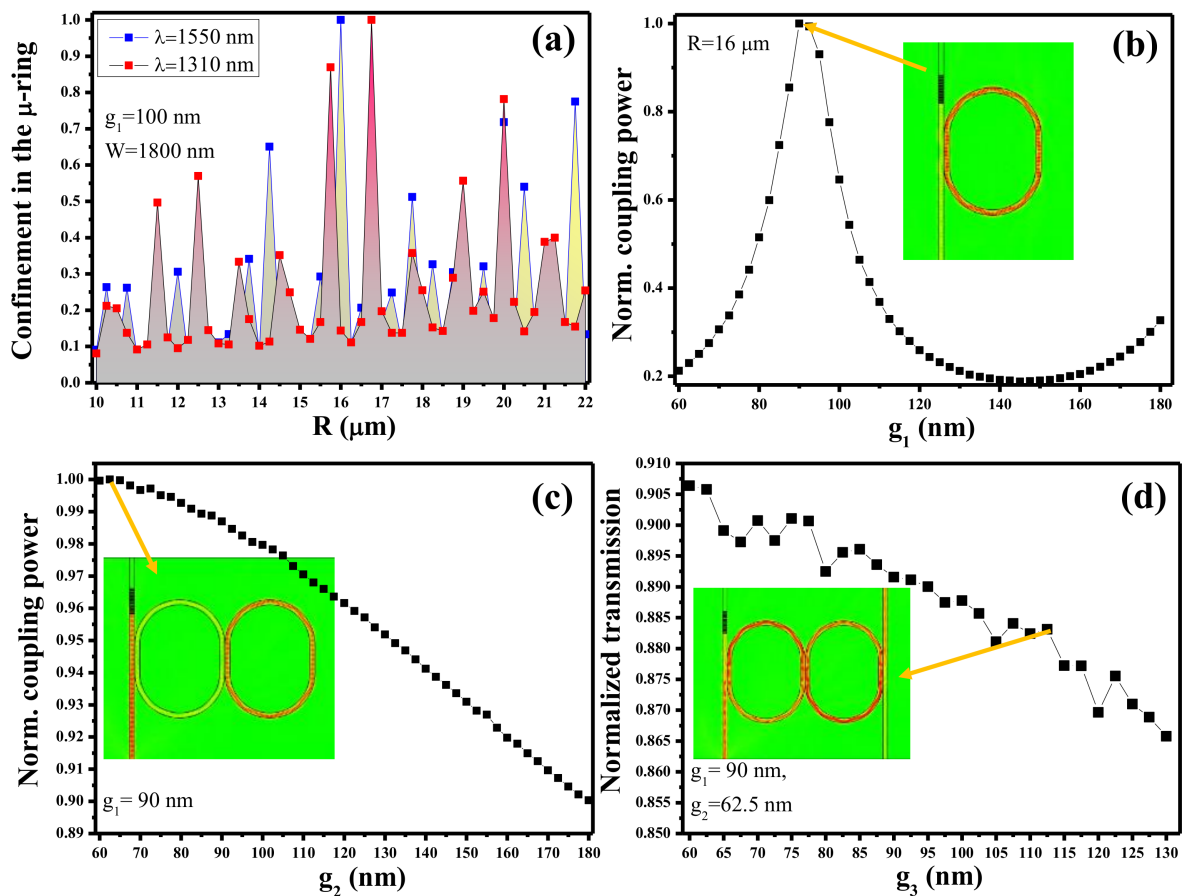
Figure 7. Optimization of the demultiplexer, (**a**) R versus E-field confinement for λ = 1310 nm and 1550 nm, (**b**) g_1 versus optimum coupling of the E-field at λ = 1550 nm in the first RTMR, (**c**) g_2 versus optimum coupling of the E-field at λ = 1550 nm in the second RTMR, (**d**) g_3 versus optimum transmission of λ = 1550 nm at output port 2.

The distance, coupling length, and refractive indices between the subsequent WGs and the microrings are the three factors that influence optical coupling. Typically, the distance between the microring and WG is reduced to maximize coupling. The coupling is also impacted by the coupling length. The coupling length denotes the length of the ring's effective curve required for the coupling phenomena to occur with the WG. Additionally, the optical coupling is influenced by the refractive indices of the materials used to make the WG, ring resonator, and medium used in between. The medium material is typically the most significant factor since it greatly influences how well light waves transmit. From Figure 7b, it can be seen that g_1 is varied between 60 nm and 180 nm, and the maximum coupling between the bus WG and a ring is obtained at g_1=90 nm. The E-field distribution in the ring at g_1 = 90 nm is indicated in the inset. The remaining geometric parameters such as R and W are fixed at 16 μm and 1800 nm, respectively.

In the next step, two rings are serially connected to the bus WG, and we aim to optimize the maximum power coupling to the second RTMR. This optimization is crucial so that most of the power can be transferred to the output WG. From Figure 7c, it can be seen that the maximum coupling in the second ring is obtained at g_2 = 62.5 nm. The E-field distribution in the structure at g_2 = 62.5 nm is shown in the inset. Now in the last step, the output WG (drop port) is side coupled to the second ring, where the coupling gap (g_3) should be optimized to obtain the maximum transmission for λ = 1550 nm. The normalized transmission of ~88% is obtained at output port 2 when g_3 = 112.5 nm and the E-distribution is revealed in the inset as shown in Figure 7d. At port 1, the normalized transmission is ~93% for the operational wavelength of 1310 nm. From these analyses, the optimized geometric parameters of the device are obtained, which are as follows: R = 16 μm, g_1 = 90 nm, g_2 = 62.5 nm, and g_3 = 112.5 nm. The CT at output port 1 and output port 2 is calculated by applying (1) and (2), respectively.

$$CT\ (dB)\ at\ output\ port\ 1 = 10 \times \log\left(\frac{P_{1550\ nm}}{P_{1310\ nm}}\right); \tag{1}$$

$$CT\ (dB)\ at\ output\ port\ 2 = 10 \times \log\left(\frac{P_{1310\ nm}}{P_{1550\ nm}}\right); \tag{2}$$

The CT of the device before the insertion of the SWG structure at output port 1 is around −1.6 dB and −9.23 dB at port 1 and port 2, respectively. The CT at port 1 is lowered to −6.6 dB by adding an SWG segment, which blocks the residual power of the 1550 nm wavelength flowing through port 1. The values of the CT with and without the SWG segment are presented in Table 2. Moreover, for the transmission bandwidth of 2 nm, the CT at Port 1 and Port 2 varies, as shown in Figures 8a and 8b, respectively. At Port 1, the CT is determined for the wavelength range of 1310 nm to 1312 nm with a step size of 0.1 nm, whereas at Port 2, the CT is also determined for the wavelength range of 1550 nm to 1552 nm with a step size of 0.1 nm.

Table 2. CT (dB) of the 1x2 demultiplexer device with and without SWG structure.

Design	Cross Talk at Output Port 1 (dB)	Cross Talk at Output Port 2 (dB)
Demultiplexer without SWG	−1.6	−9.23
Demultiplexer with SWG	−6.6	−9.04
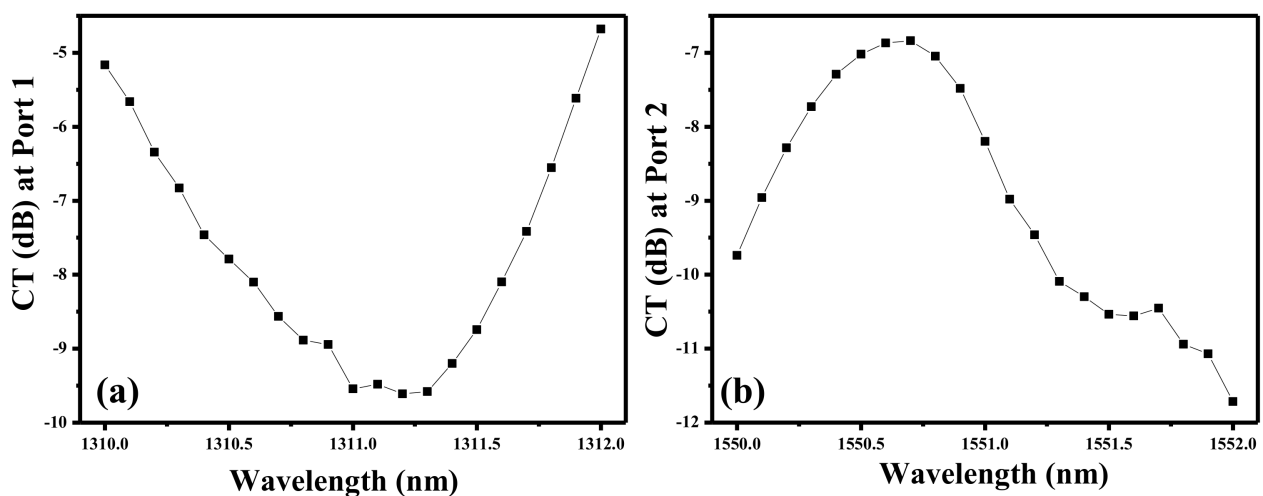
Figure 8. CT at Port 1 and Port 2 for the operational wavelength of: (**a**) 1310 nm to 1312 nm, (**b**) 1550 nm to 1552 nm.

The normalized E-field distribution for λ = 1310 nm and λ = 1550 nm is plotted in Figure 9a,b, respectively. It can be seen that when λ = 1310 nm is launched at the input port, it travels through the bus WG without coupling to the ring as it does not satisfy the resonance condition. Whereas λ = 1550 nm is launched at the input port coupled to the first ring as it satisfies the coupling condition, and then the mode power is transferred at output port 2 after passing through the second RTMR. For comparison, several demultiplexer designs established on different platforms and their performance are presented in Table 3.
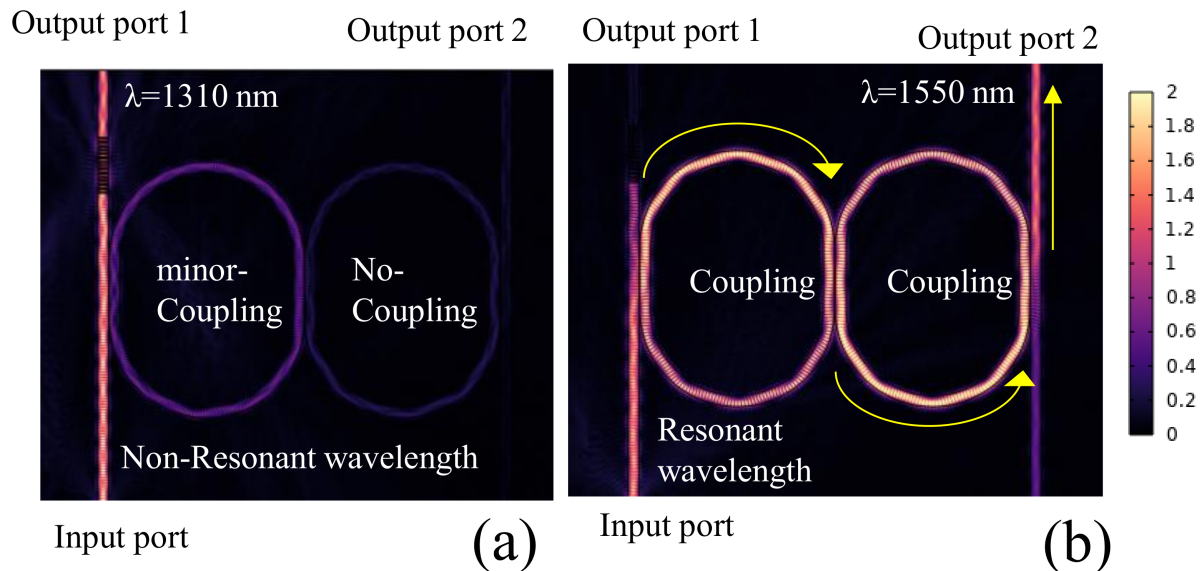
Figure 9. Normalized E-field distribution in the 1 × 2 demultiplexer design at the operational wavelength of: (**a**) 1310 nm, and (**b**) 1550 nm.

Table 3. Comparison of the proposed demultiplexer design with the previously published demultiplexers.

Ref.	Material	Design	Wavelength (nm)	Numerical/ Experimental	CT (dB)	Footprint
[23]	GaN, Si	MMI	1530–1565	Numerical	−19.97 to −13.77	-
[24]	GaN, Si	MMI	547–584	Numerical	13.8–18.3 dB	-
[25]	Si	PhC, RR	1535–1539	Numerical	−18.31	-
[26]	Si	RR	1550–1567	Numerical	−13−−24	689.61 (μm^2)
[27]	SOI	SWG	1310, 1550	Numerical	-	-
[28]	SOI	SWG	1310, 1550	Experimental	-	-
[29]	SOI	SWG	1310, 1550	Numerical	-	-
[30]	SOI	AWG	1500–1570	Experimental	-	110 × 93 (mm^2)
[31]	Si3N$_4$	MZI	1530–1580	Experimental	14.5	-
This work	SiO$_2$:TiO$_2$	RR	1550, 1310	Numerical	−6.6 and −9.04	84 μm × 125 μm

5. Conclusions

Herein, a 1 × 2 demultiplexer for telecommunication wavelengths 1310 nm and 1550 nm is proposed on a silica-titania platform. The choice of this platform is due to its highly attractive optical, physical, and chemical characteristics. The numerical analysis of the device is conducted via a finite element method. Two serially cascaded racetrack microrings (RTMRs) are side coupled to a bus WG to launch the input light. The wavelength division multiplexing (WDM) is achieved in such a configuration and the separated signals are collected via the thru port and drop port. Additionally, a subwavelength grating (SWG) structure is incorporated in the thru port to reduce the CT between the output ports. The minimum CT of −6.6 dB and −9.04 dB is obtained for 1550 nm and 1310 nm, respectively. This study can further open the possibilities of designing 1 × N demultiplexing devices, which can enhance the number of channels in communication systems.

Conflicts of Interest: The authors declare no conflict of interest.

References

1. Sheng, Y.-B.; Zhou, L.; Long, G.-L. One-step quantum secure direct communication. *Sci. Bull.* **2022**, *67*, 367–374. [CrossRef] [PubMed]
2. Khonina, S.; Kazanskiy, N.; Butt, M.; Karpeev, S. Optical multiplexing techniques and their marriage for on-chip and optical fiber communication: A review. *Opto-Electron. Adv.* **2022**, *5*, 210127. [CrossRef]
3. Park, J.; Joo, J.; Kwack, M.-J.; Kim, G.; Han, S.-P.; Kim, S. Three-dimensional wavelength-division multiplexing interconnects based on a low-loss SixNy arrayed waveguide grating. *Opt. Express* **2021**, *29*, 35261–35270. [CrossRef]
4. Pathak, S.; Thourout, D.; Bogaerts, W. Comparison of AWGs and Echelle gratings for wavelength division multiplexing on silicon-on-insulator. *IEEE Photonics J.* **2014**, *6*, 4900109. [CrossRef]
5. Lin, Y.-J.; Lee, S.-L.; Yao, C.-L. Four-channel coarse-wavelength division multiplexing demultiplexer with a modified Mach-Zehnder interferometer configuration on a silicon-on-insulator waveguide. *Appl. Opt.* **2003**, *42*, 2689–2694. [CrossRef] [PubMed]
6. Ahmmed, K.; Chan, H.; Li, B. Three-mode multiplexer and demultiplexer based on the Mach-Zehnder interferometer. *OSA Contin.* **2021**, *4*, 1519–1532. [CrossRef]
7. Menahem, J.; Malka, D. 1×4 wavelength demultiplexer C-band using cascaded multimode interference on SiN buried waveguide structure. *Materials* **2022**, *15*, 5067. [CrossRef]
8. Rouifed, M.-S.; Littlejohns, C.; Tina, G.; Qiu, H.; Penades, J.; Nedeljkovic, M.; Zhang, Z.; Liu, C.; Thomson, D.; Mashanovich, G.; et al. Ultra-compact MMI-based beam splitter demultiplexer for the NIR/MIR wavelengths of 1.55 um and 2 um. *Opt. Express* **2017**, *25*, 10893–10900. [CrossRef]
9. Chen, J.; Zhang, Y.; Shi, Y. An on-chip triplexer based on silicon Bragg grating-assisted multimode interference couplers. *IEEE Photon. Technol. Lett.* **2017**, *29*, 63–65. [CrossRef]
10. Xu, Y.; Zhou, W.; Chen, K.; Huang, X. Y-branch wavelength demultiplexer based on topological valley photonic crystals. *Opt. Laser Technol.* **2022**, *155*, 108422. [CrossRef]
11. Prajzler, V.; Mastera, R. Wavelength division multiplexing module with large core optical polymer planar splitter and multilayered dielectric filters. *Opt. Quantum Electron.* **2017**, *49*, 133. [CrossRef]
12. Mehdizadeh, F.; Soroosh, M.; Alipour-Banaei, H. An optical demultiplexer based on photonic crystal ring resonators. *Optik* **2016**, *127*, 8706–8709. [CrossRef]
13. Masilamani, S.; Punniakodi, S. Photonic crystal ring resonator based optical MUX/DEMUX design structures: A survey and comparison study. *J. Opt.* **2020**, *49*, 168–177. [CrossRef]
14. Rakshit, J.; Roy, J. All-optical ultrafast switching in a silicon microring resonator and its application to design multiplexer/demultiplexer, adder/substrator and comparator circuit. *Opt. Appl.* **2016**, *XLVI*, 517.
15. Bagheri, A.; Nazari, F.; Moravvej-Farshi, M. Tunable optical demultiplexer for dense wavelength division multiplexing systems using graphene-silicon microring resonators. *J. Electron. Mater.* **2020**, *49*, 7410–7419. [CrossRef]
16. Chang, H.; Kuo, Y.; Jones, R.; Barkai, A.; Bowers, J. Integrated hybrid silicon triplexer. *Opt. Express* **2010**, *18*, 23891–23899. [CrossRef]
17. Xu, H.; Shi, Y. On-chip silicon triplexer based on asymmetrical directional couplers. *IEEE Photon. Technol. Lett.* **2017**, *29*, 1265–1268. [CrossRef]
18. Zhu, N.; Song, J.; Wosinski, L.; He, S.; Thylen, L. Experimental demonstration of a cross-order echelle grating triplexer based on an amorphous silicon nanowire platform. *Opt. Lett.* **2009**, *34*, 383–385. [CrossRef]

19.   Butt, M.; Kazanskiy, N.; Khonina, S. Miniaturized design of a 1 × 2 plasmonic demultiplexer based on metal-insulator-metal waveguide for telecommunication wavelengths. *Plasmonics* **2023**. [CrossRef]

20.   Xie, Y.-M.; Lu, Y.-S.; Weng, C.-X.; Cao, X.-Y.; Jia, Z.-Y.; Bao, Y.; Wang, Y.; Yin, H.-L.; Chen, Z.-B. Breaking the rate-loss bound of quantum key distribution with asynchronous two-photon interference. *PRX Quantum* **2022**, *3*, 020315. [CrossRef]

21.   Gu, J.; Cao, X.-Y.; Fu, Y.; He, Z.-W.; Yin, Z.-J.; Yin, H.-L.; Chen, Z.-B. Experimental measurement-device-independent type quantum key distribution with flawed and correlated sources. *Sci. Bull.* **2022**, *67*, 2167–2175. [CrossRef] [PubMed]

22.   Wu, J.; Long, G.-L.; Hayashi, M. Quantum Secure Direct Communication with Private Dense Coding Using a General Preshared Quantum State. *Phys. Rev. Appl.* **2022**, *17*, 064011. [CrossRef]

23.   Zaken, B.; Baruch, B.; Zanzury, T.; Malka, D. An 8-channel wavelength MMI demultiplexer in slot waveguide structures. *Materials* **2016**, *9*, 881. [CrossRef] [PubMed]

24.   Tamir, S.; Karanov, N.; Malka, D. 1 × 4 MMI visible light wavelength demultiplexer based on a GaN slot-waveguide structure. *Photonics Nanostruct.-Fundam. Appl.* **2018**, *30*, 45–49.

25.   Dhandrapati, L.; Tupakula, S. A novel 8-channel DWDM demultiplexer on silicon photonic crystal slab: Design and analysis. *Optik* **2022**, *256*, 168734. [CrossRef]

26.   Naghizade, S.; Sattari-Esfahlan, S. An optical five channel demultiplexer-based simple photonic crystal ring resonator for WDM applications. *J. Opt. Commun.* **2020**, *41*, 37–43. [CrossRef]

27.   Chen, J. A broadband wavelength demultiplexer assisted by SWG-based directional couplers. *Optik* **2020**, *202*, 163602. [CrossRef]

28.   Wang, F.; Xu, X.; Zhang, C.; Sun, C.; Zhao, J. Design and demonstration of compact and broadband wavelength demultiplexer based on subwavelength grating (SWG). *IEEE Photonics J.* **2022**, *14*, 1–6. [CrossRef]

29.   Hao, T.; Sánchez-Postigo, A.; Cheben, P.; Ortega-Moñux, A.; Winnie, N.Y. Dual-band polarization-independent subwavelength grating couplers for wavelength demultiplexing. *IEEE Photonics Technol. Lett.* **2020**, *32*, 1163–1166. [CrossRef]

30.   Fukazawa, T.; Fumiaki, O.; Toshihiko, B. Very compact arrayed-waveguide-grating demultiplexer using Si photonic wire waveguides. *Jpn. J. Appl. Phys.* **2004**, *43*, L673. [CrossRef]

31.   Hai, M.S.; Leinse, A.; Veenstra, T.; Liboiron-Ladouceur, O. A thermally tunable 1 × 4 channel wavelength demultiplexer designed on a low-loss Si3N4 waveguide platform. *Photonics* **2015**, *2*, 1065–1080. [CrossRef]

32.   Butt, M.A.; Kaźmierczak, A.; Tyszkiewicz, C.; Karasiński, P.; Środa, E.; Olszewski, J.; Pala, P.; Martynkien, T.; Hlushchenko, D.; Baraniecki, T.; et al. HYPHa project: A low-cost alternative for integrated photonics. *Photonics Lett. Pol.* **2022**, *14*, 25–27. [CrossRef]

33.   Kozlowski, L.; Shahbaz, M.; Butt, M.; Tyszkiewicz, C.; Karasiński, P.; Kazmierczak, A.; Piramidowicz, R. Low-cost Integrated Photonic Platform Developed via a Sol-gel Dip-coating Method: A Brief Review. *Sens. Transducers* **2022**, *259*, 82–92.

34.   Butt, M.; Tyszkiewicz, C.; Wojtasik, K.; Karasinski, P.; Kazmierczak, A.; Piramidowicz, R. Subwavelength grating waveguide structures proposed on the low-cost silica-titania platform for optical filtering and refractive index sensing applications. *Int. J. Mol. Sci.* **2022**, *23*, 6614. [CrossRef]

35.   Karasinski, P. Sol-gel derived optical waveguide films for planar sensors with phase modulation. *Opt. Appl.* **2004**, *34*, 467–475.

36.   Karasinski, P.; Jaglarz, J.; Mazur, J. Low loss silica-titania waveguide films. *Photonics Lett. Pol.* **2010**, *2*, 37–39.

37.   Racka-Szmidt, K.; Stonio, B.; Zelazko, J.; Filipiak, M.; Sochacki, M. A review: Inductively coupled plasma reactive ion etching of silicon carbide. *Materials* **2022**, *15*, 123. [CrossRef] [PubMed]

38.   Park, H.; Cho, J.; Jung, J.; Duy, P.P.; Le, A.; Yi, J. A review of wet chemical etching of glasses in hydrofluoric acid based solution for thin film silicon solar cell application. *Curr. Photovolt. Res.* **2017**, *5*, 75–82.

39.   Chen, Y.; Shu, Z.; Zhang, S.; Zeng, P.; Liang, H.; Zheng, M.; Duan, H. Sub-10 nm fabrication: Methods and applications. *Int. J. Extrem. Manuf.* **2021**, *3*, 032002. [CrossRef]

40.   Kazanskiy, N.L.; Butt, M.; Khonina, S.N. Silicon photonic devices realized on refractive index engineered subwavelength grating waveguides-A review. *Opt. Laser Technol.* **2021**, *138*, 106863. [CrossRef]

41.   Khonina, S.N.; Kazanskiy, N.L.; Butt, M.A. Spectral characteristics of broad band-rejection filter based on Bragg grating, one-dimensional photonic crystal, and subwavelength grating waveguide. *Phys. Scr.* **2021**, *96*, 055505. [CrossRef]